JACS
JOURNAL OF THE AMERICAN CHEMICAL SOCIETY
Article
pubs.acs.org/JACS

Multifunctional Mesoporous Silica-Coated Graphene Nanosheet Used for Chemo-Photothermal Synergistic Targeted Therapy of Glioma

Yi Wang,[‡] Kaiyuan Wang,[§] Jianfeng Zhao,[‡] Xingang Liu,[‡] Juan Bu,[⊥] Xueying Yan,[§] and Rongqin Huang*[,†,⊥]

[†]Department of Pharmaceutics, School of Pharmacy, Key Laboratory of Smart Drug Delivery, Ministry of Education and PLA, Fudan University, Shanghai 201203, China

[‡]Center of Analysis and Measurement, Fudan University, Shanghai 200433, China

[§]School of Pharmacy, Heilongjiang University of Chinese Medicine, Harbin 150040, China

[⊥]Department of Macromolecular Science, State Key Laboratory of Molecular Engineering of Polymers, Fudan University, Shanghai 200433, China

Supporting Information

ABSTRACT: Current therapy of malignant glioma in clinic is unsatisfactory with poor patient compliance due to low therapeutic efficiency and strong systemic side effects. Herein, we combined chemo-photothermal targeted therapy of glioma within one novel multifunctional drug delivery system. A targeting peptide (IP)-modified mesoporous silica-coated graphene nanosheet (GSPI) was successfully synthesized and characterized, and first introduced to the drug delivery field. A doxorubicin (DOX)-loaded GSPI-based system (GSPID) showed heat-stimulative, pH-responsive, and sustained release properties. Cytotoxicity experiments demonstrated that combined therapy mediated the highest rate of death of glioma cells compared to that of single chemotherapy or photothermal therapy. Furthermore, the IP modification could significantly enhance the accumulation of GSPID within glioma cells. These findings provided an excellent drug delivery system for combined therapy of glioma due to the advanced chemo-photothermal synergistic targeted therapy and good drug release properties of GSPID, which could effectively avoid frequent and invasive dosing and improve patient compliance.

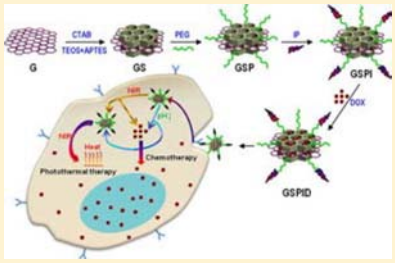

INTRODUCTION

Malignant glioma is considered to be one of the most aggressive tumors and the major cause of death among brain disorders.[1] Chemotherapy, alone or combined with radiotherapy, is still the standard treatment after surgical resection.[2] However, the prognosis remains extremely poor with median overall survival less than 2 years.[3] This might be mainly attributed to the fact that current chemotherapy lacks specificity and leads to undesired, adverse effects to normal tissues and insufficient dosage to diseased regions. Thus, chemo-photothermal synergistic targeted therapy of glioma would be a practical and efficient solution worthy to be tried. On one hand, targeted drug delivery can enhance the tumor accumulation of antitumor drugs and decrease side effects. On the other hand, photothermal therapy, a minimally invasive treatment, can increase the sensitivity of chemotherapy and synergistically improve the therapeutic effects.

To avoid complex administration and improve patient compliance, it is highly desired that a good drug delivery system possesses both the chemo- and photothermal therapeutic functions. Graphene nanosheet, due to its biocompatibility, unique structure, and relatively low cost, has now attracted great attention from scientific communities. It is an emerging vector which has been demonstrated to efficiently deliver water-insoluble cancer drugs,[4] proteins,[5] gene medicines,[6] and bioimaging agents[7] into cells. Most importantly, graphene nanosheet is a photosensitizer with high absorption in the near-infrared (NIR)and shows potential ability for photothermal therapy in vitro and in vivo.[8−10] However, some shortcomings including insolubility and difficulty for interfacial interaction with the targeting matrix greatly limit its biomedical applications.[11] Furthermore, graphene nanosheet mainly absorbs insoluble molecules via noncovalent binding such as $\pi-\pi$ interaction,[12] with low drug loading efficiency. Recently, the mesoporous silica-coated graphene nanosheet (GS) has emerged as a novel material.[13] As is known, mesoporous silica nanoparticles themselves are good vectors for insoluble chemotherapeutic drugs.[14,15] A vertical coating of mesoporous silica on a graphene nanosheet could improve the interfacial properties of graphene and integrate the advantages of both materials as drug delivery vectors. These advantages include (1) enlarging the surface area, (2) enhancing the hydrophilicity and dispersity, (3) being more easily covalently functionalized, and

Received: December 19, 2012
Published: March 15, 2013

   dx.doi.org/10.1021/ja312221g | J. Am. Chem. Soc. 2013, 135, 4799−4804

Scheme 1. Design of GSPID As a Multifunctional Drug Delivery System for Combined Chemo-Photothermal Targeted Therapy of Glioma

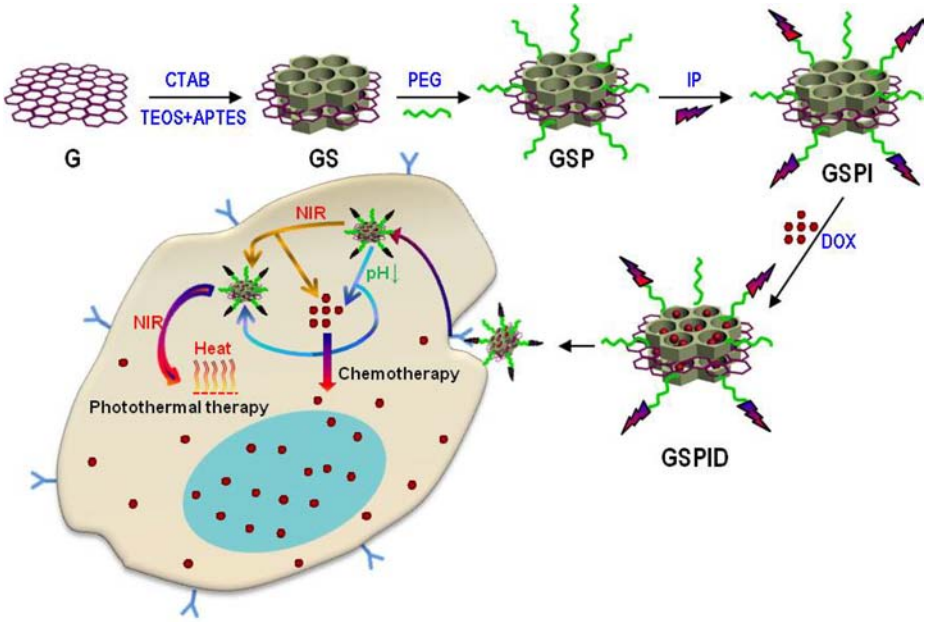

(4) achieving high drug loading efficiency via both $\pi-\pi$ stacking and pore adsorption. Therefore, GS was explored as the bifunctional vector for chemo-photothermal therapy in this work.

Active targeting technique is a promising pathway to enhance the glioma accumulation of drug carriers including GS. Receptor-mediated glioma-targeting drug delivery has been achieved via different ligands including small molecules,[16] peptides,[17] and proteins,[18] binding to corresponding receptors. It has been reported that receptor chain 2 of interleukin 13 (IL-13Rα2) is overexpressed in a series of malignant tumors including glioma, ovarian cancer, head and neck cancer, and renal cell carcinoma, but is scarcely found in normal tissues derived from same organs.[15,19] The natural ligand with high affinity to IL-13Rα2, interleukin 13, thus was explored for constructing glioma-targeting drug delivery systems.[20] However, direct usage of interleukin 13 suffers from problems such as hard manipulation and easy denaturation. In our previous research, a peptide corresponding to the residues within interleukin 13, designated as IP, was first exploited as a glioma-targeting ligand to modify mesoporous silica nanoparticles.[15] The results demonstrated that IP conjugation could significantly enhance the cellular uptake of the drug delivery system in U251 cells but not in normal astrocyte 1800 cells, indicating good glioma-targeting capability of IP.[15]

Herein, an IP-conjugated GS-based drug delivery system was designed for synergistic targeted chemo-photothermal therapy of glioma, the detailed illustration of which is shown in Scheme 1.

RESULTS AND DISCUSSION

GS was successfully synthesized and well characterized. Modified Hummer's method[21] assisted with repeated ultrasonication and centrifugation was used to synthesize single-layer graphene oxide (GO) nanosheet with a lateral size around 50–250 nm (Figure S1A Supporting Information [SI]). GS was prepared by hydrothermal reaction of CTAB, TEOS, APTES, and GO (see the Experimental Details). The XRD pattern (Figure 1A) showed that GS had a hexagonal array of pores and an ordered structure. The lattice parameter (a_0) calculated from the diffraction peaks (100) was 4.69 nm. The results of N_2 adsorption–desorption isotherm and pore size distribution cure (Figure 1B) indicated that GS possessed large BET surface area (1252 m^2/g), pore volume (1.27 cm^3/g), and uniform pore

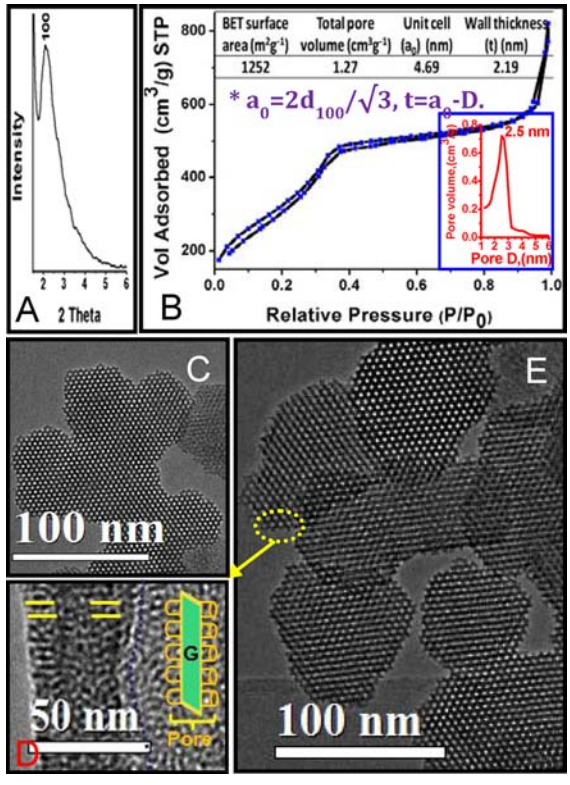

Figure 1. (A) Small-angle XRD pattern; (B) N_2 adsorption–desorption isotherm and pore size distribution curve (inset); (C, D, E) HRTEM and TEM images of GS.

dx.doi.org/10.1021/ja312221g | J. Am. Chem. Soc. 2013, 135, 4799–4804

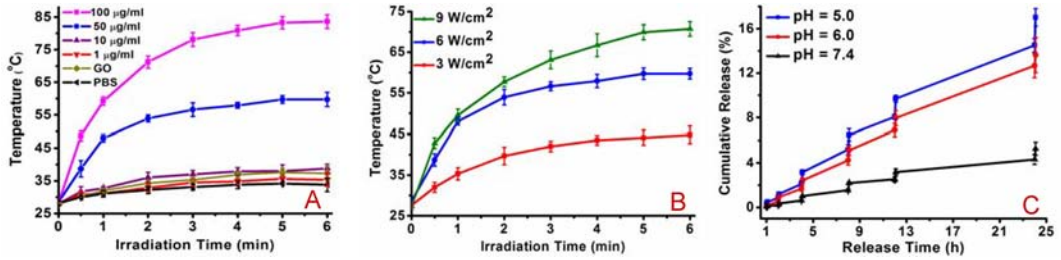

Figure 2. (A) Photothermal heating curves of GSPI solution at various GS concentrations at the power intensity of 6 W/cm^2. The GO solution has the same graphene concentration to GSPI solution with GS concentration at 50 μg/mL. (B) Photothermal heating curves of GSPI at various power intensities with GS concentration at 50 μg/mL. (C) Cumulative release profiles of DOX from GSPID at different pHs with 6 W/cm^2 NIR irradiation. Data are expressed as mean ± SEM (n = 3).

diameter (D) of 2.5 nm. The calculated wall thickness ($t = a_0 - D$) of mesopores reached 2.19 nm. TEM images (Figure 1C,E and Figure S1B,C, SI) well illustrate the existing mesopores on GS with the lateral size around 50−150 nm, smaller than the added GO nanosheet due to the hydrothermal cutting and sonication. Of much interest was that the mesopores on the GS were perpendicular to the graphene nanosheet as observed from the HRTEM images in Figure 1D, and the pore depth was about 25 nm. In addition, the existence of graphene between the mesoporous silica was proved by the Raman spectra (Figure S2A in the SI) which gave obvious signals similar to those of defective graphene.[22] Thermogravimetric-differential thermogravimetric (TG-DTG) analysis (Figure S2B in the SI) also showed that approximately 35% weight loss (decomposition of graphene) happened around 500 °C.[22] FT-IR spectra (Figure S3A, SI) indicated the added GO was reduced during the alkaline hydrothermal coating of mesoporous silica.[23]

GS was modified with hydrophilic polyethylene glycol (PEG) (GSP) and then further conjugated by IP (GSPI). The successful PEGylation and IP modification for GS was also characterized by FT-IR spectra (Figure S3A, SI).[15] The prepared materials were also investigated by zeta (ζ) potential analysis. The ζ potential of GS (−26.3 mV) was much smaller than that of GO (−52.2 mV) due to the deoxidization of electronegative groups on GO such as hydroxyl and carboxyl during silica coating. After PEGylation, the ζ potential decreased to −38.3 mV and then increased to −22.4 mV after modification of electropositive IP. The loading of DOX inside the pores did not greatly change the ζ potential (−20.1 mV). The dispersity experiment showed that the water-soluble GO would aggregate after being deoxidized, while GS retained water dispersion via coating of the hydrophilic mesoporous silica. The PEGylation and IP modification made the materials much more dispersible (Figure S4 in the SI).

As shown in the UV−vis spectrum, GS had remarkably higher NIR absorbance than GO (Figure S3B, SI). PEGylation and IP modification could further enhance the NIR absorbance, where GSPI obtained the highest one. The increased absorption may be attributed to the enhanced dispersity of GSP/GSPI solutions and the further reduction of GS during the PEG/IP functionalization.[24] When irradiated by an 808 nm NIR laser at the power intensity of 6 W/cm^2, the solution temperature exceeded 50 °C within 2 min at the GS concentration of 50 μg/mL (Figure 2A). In strong contrast, the GO solution under the same laser irradiation remained below 37 °C within 6 min (Figure 2A). Furthermore, the photothermal heating effect of GSPI exhibited a concentration-dependent (with GS concentration from 1 to 100 μg/mL, Figure 2A) and laser power intensity-dependent (from 3 to 9 W/cm^2, Figure 2B) manner. The superior photothermal efficiency of GSPI, even better than that of carbon nanotubes,[25] has potential for thermal ablation of malignant tissues. On the other hand, when GSPI loaded the chemotherapeutic drug doxorubicin (DOX), yielding GSPID, the photothermal heating effect of GSPI could promote the release of DOX. The NIR irradiation apparently enhanced the cumulative release of DOX at different time points and pHs (Figure 2C) due to heat stimulative dissociation of the strong interactions between DOX and GSPI including $\pi-\pi$ stacking and pore adsorption. Taking pH 5.0 for example, the cumulative release of DOX (17%) with NIR irradiation was about 3-fold greater than that without NIR irradiation (5.9%) (Figure 2C and Figure S5 in the SI). That means the photothermal effect of GSPI could significantly increase the sensitivity of chemotherapy. Also shown in Figure 2C and Figure S5, SI, the release of DOX exhibited a pH-responsive pattern, whereas a higher cumulative DOX release was achieved in relation to a lower pH. The phenomenon can be attributed to the reduction of the hydrophobic interaction between DOX and graphene[26] and also the decrease of electrostatic interaction between DOX and mesoporous silica.[27] It has been reported that the tumor microenvironment is mildly acidic with a pH range of 5.8−7.1[28] and the intracellular environment is even more acidic, at ∼5.0 pH.[29] The pH-sensitive and NIR-stimulative release of DOX can greatly enhance the therapeutic effect, based on the targeting accumulation of GSPID within the glioma.

In order to evaluate the therapeutic effect of GSPID, cell viability with different treatments was measured. The qualitative results obtained with confocal microscopy showed that GSPID with NIR irradiation mediated the highest rate of cell death compared to a single treatment of GSPID (chemotherapy) or GSPI with NIR irradiation (photothermal therapy) (Figure 3A−D). Limited death was observed by GSPID treatment alone (Figure 3C), which could be due to insufficient release of DOX within 30 min. When the incubation time was extended to 2 h, the quantitative evaluation of cell viability was performed via the Cell Counting Kit-8 (CCK-8) assay (Figure 3E). The IC_{50} of each treatment is shown in Table 1, and the combination index (CI) was calculated to evaluate the combination effect of different therapies.[30] In this work, the CI value was 0.504 (<1), which demonstrated the synergistic effect of GSPID chemotherapy and photothermal therapy. Herein we can see that, although the cumulative release of DOX was less than 1% at the 2 h point, there still existed apparent cytotoxicity to U251 glioma cells (Figure 3 and Table 1). The main reason can be attributed to the high DOX loading efficiency of GSPID (about 1.27 ± 0.11 μg DOX/μg GS), in which the aromatic DOX molecule can be stored in mesopores

dx.doi.org/10.1021/ja312221g | J. Am. Chem. Soc. 2013, 135, 4799−4804

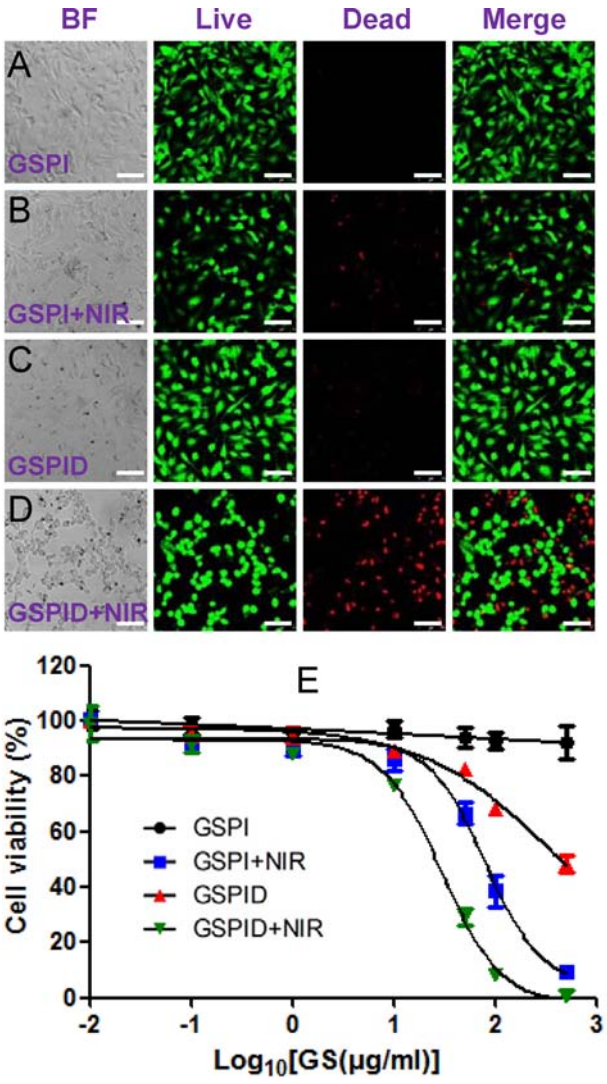

Figure 3. Cytotoxicity of U251 glioma cells under different treatments. (A–D) Confocal microscopy of glioma cells via LIVE-DEAD staining. BF: bright field images. Green: live cells. Red: dead cells. Bar = 75 μm. (E) Cell viability profiles of glioma cells.

Table 1. IC_{50} (μg/mL) in Glioma Cells under Different Treatments and the Calculated CI Value

GSPI	GSPI + NIR	GSPID	GSPID + NIR		CI
GS	GS	DOX	GS	DOX	
1.139×10^{30}	78.78	398.15	29.49	37.45	0.504

via electrostatic interaction and adsorbed on graphene via supramolecular π stacking.[26] When the incubation time was prolonged, more severe toxicity could be observed due to more drug release within glioma cells. It has been reported that graphene might cause cell death via generation of reactive oxygen species (ROS).[31] However, this effect would be compromised via the coating of mesoporous silica.[32] As shown in Figure 3A and E and Table 1, no apparent toxicity was observed using GSPI material without NIR irradiation, indicating that alteration of ROS level might not be the chief mechanism. The exciting information integrated from the in vitro release and cell viability results (Figure 2C and Figure 3) demonstrated that (1) GSPID is a great sustained release system, and (2) the slowly released DOX is sufficient for the synergistic chemo-photothermal therapy. This would favor the long and continued therapy of glioma without frequent dosing, and improve the patients' compliance.

For biomedical applications of graphene-based materials, an important issue is the long-term toxicity in vivo. Graphene oxide without any functionalization could induce undesirable toxicity including thromboembolism in systemic circulation.[33] Appropriate surface modification such as PEGylation and amination could significantly reduce these untoward effects.[34−36] In our work, graphene oxide was reduced during the alkaline hydrothermal coating of mesoporous silica, and amination by the treatment of APTES. Moreover, PEGylation was applied to enhance the biocompatibility and further reduce the in vivo toxicity. Thus, the designed GS-based system was speculated to be relatively safe for in vivo application, which would be carefully examined in future studies.

Finally, the targeting ability of GSPID was evaluated using the IP-unmodified counterpart (GSPD) as control. Measurement of cellular uptake via confocal microscopy was carried out for qualitative evaluation, and cell viability measured via CCK-8 analysis was performed for quantitative evaluation. The higher cytotoxicity reflects the higher cellular uptake to some extent. As shown in Figure 4, GSPID exhibited significantly higher cellular uptake and cytotoxicity in glioma cells but had no apparent effect on normal cells, compared to GSPD. Since the major distinction of GSPID and GSPD is the IP modification, the targeting property of IP was verified.

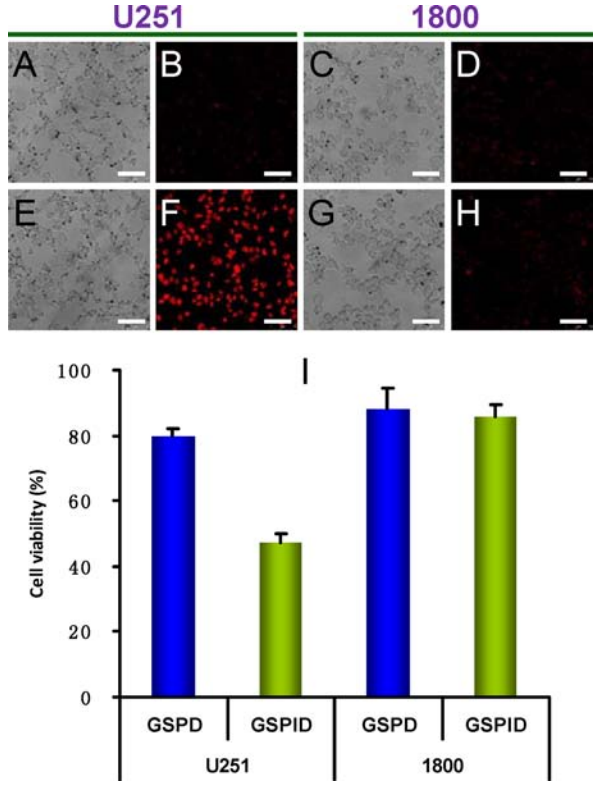

Figure 4. Targeting evaluation of GSPID. Confocal microscopy images of GSPD (A–D) and GSPID (E–H) incubated with U251 cells and 1800 cells for 30 min. A, C, E, G are the corresponding bright field images of fluorescent images B, D, F, and H. Red: DOX. Bar = 75 μm. (I) Cytotoxicity of GSPD and GSPID incubated with U251 cells and 1800 cells for 6 h.

dx.doi.org/10.1021/ja312221g | J. Am. Chem. Soc. 2013, 135, 4799–4804

As is known, glioma is a type of deep-seated tumor within the brain. Effective photothermal therapy of glioma requires NIR light to penetrate through the skull into the diseased tissue. This feasibility has been demonstrated by recent reports where efficient photothermal therapy was achieved in orthotopic murine glioma models using 808-nm NIR lasers.[37,38]

CONCLUSION

In summary, a novel multifunctional drug delivery system, GSPID, was successfully constructed for synergistic chemo-photothermal therapy. GSPID possesses the following properties, (1) adsorption of antitumor drug DOX with a high loading efficiency for chemotherapy, (2) high absorption in the NIR window and efficient heat transformation for photothermal therapy, (3) targeting accumulation within glioma cells via IP conjugation, and (4) excellent release characteristics including heat-stimulative, pH-responsive, and sustained release. Various functions were smartly concentrated on one drug delivery system, which could effectively avoid frequent and invasive dosing. Thus, GSPID would be a potential platform for biomedical application.

EXPERIMENTAL DETAILS

Materials. IL-13 peptide (IP) was synthesized by Ziyu Biotechnology Co., Ltd. (Shanghai, China).[15] α-Malemidyl-ω-*N*-hydroxysuccinimidyl polyethyleneglycol (NHS-PEG-MAL, MW 3500) was obtained from JenKem Technology Co., Ltd. (Beijing, China). Doxorubicin (DOX) was purchased from Huafeng United Technology Co., Ltd. (Beijing, China). Cetyltrimethylammonium bromide (CTAB) was purchased from Mingzhi Chemical Co. (Shanghai, China). Cell Counting Kit-8 (CCK-8) was obtained from Dojindo Laboratories (Japan). LIVE-DEAD Kits were purchased from Molecular Probes (Eugene, OR, U.S.A.). Dulbecco's Modified Eagle Medium (DMEM) and fetal bovine serum (FBS) were purchased from Gibco (Tulsa, OK, U.S.A.). Tetraethyl orthosilicate (TEOS), aminopropyltriethoxysilane (APTES), and other reagents, if not specified, were purchased from Sigma-Aldrich (St. Louis, MO, U.S.A.). All the chemicals were used without further purification.

Synthesis and Preparation of Drug Delivery Systems. Graphene oxide (GO) nanosheet was prepared by a modified Hummer's method.[21] In order to cut the nanosheet into small pieces, the GO solution was sonicated for 1 h (600 W) and hydrothermally treated, then centrifuged (16,000 rpm) for 30 min. This process was repeated for three times, and the supernatant was saved. For the synthesis of GS, CTAB and $NaBH_4$ solution (1 mg/mL) was mixed with GO nanosheet solution (0.2 mg/mL). The mixture was stirred at 60 °C for 30 min, and then aqueous NaOH (0.2 M) was added. The solution continued to stir for 15 min after which was hydrothermal treatment for 24 h. The black aqueous dispersion was obtained by sonication for 1 h. Subsequently, the prepared mixed solution of APTES, ethanol, and TEOS was dropped slowly into the black aqueous dispersion under stirring. After that, the mixture was reacted under 100 °C for 24 h. Finally, the solid product was recovered by centrifugation and washing. To remove the large aggregation, GS solution was sonicated (160 W, 30 min) and centrifuged (3000 rpm, 3 min), and the suspension was recovered. To remove the surfactants from the pores, GS was repeatedly refluxed in a mixture of methanol and NH_4NO_3.

For the synthesis of PEGylated GS (GSP), GS (0.5 mg/mL) was mixed with bifunctional PEG (2 mg/mL) for 2 h in phosphate-buffered solution (PBS, pH 8.0). The product GSP was recovered by centrifugation at 10,000 rpm for 5 min and dispersed into PBS (pH 7.0) by sonication; IP (0.5 mg/mL) was then added. After stirring for 24 h, the resulting IP-modified conjugate (GSPI) was also purified via centrifugation. To load DOX, the GS-based vectors were soaked, sonicated, and stirred in a DOX/methanol solution (1 mg/mL). After 24 h, the mixture was centrifuged, and the supernatant was removed. The DOX-loaded drug delivery systems (GSPD and GSPID) were dried under vacuum to remove trace methanol. After that, the systems were rinsed with PBS (pH 7.4) to remove DOX that was adsorbed on the surface. Finally, they were resuspended in PBS (pH 7.4) at the proper concentration.

Characterization of Synthesized GS. X-ray diffraction patterns (XRD) were obtained from a Rigaku D/MAX-RB diffractometer using Cu Kα radiation at 40 kV and 100 mA. Nitrogen adsorption−desorption isotherms at the temperature of liquid nitrogen and pore size distribution curves were measured using Tristar 3000 systems. The measurements were performed after the samples were outgassed for more than 5 h at 150 °C. To observe the detailed morphology of GS, transmission electron microscopy (TEM) was performed on JEOL JEM-2010 instruments with an acceleration voltage of 200 kV.

Loading Efficiency Measurement. The adsorption measurements of the original solution and the supernatant were recorded to determine the amount of DOX that was loaded in GSPI, and the loading efficiency was calculated. For the measurement, the standard curve was established. The fluorescent signals of DOX (excitation at 488 nm and emission at 600 nm) were recorded using a Cary Eclipse fluorescence spectrophotometer (Varian, U.S.A.).

Photothermal Heating Effect of GSPID. To determine the impact of material concentrations on the photothermal heating effect, a series of solutions of GSPI in PBS (pH 7.4) with different GS concentrations from 1 to 100 μg/mL were irradiated by NIR laser (wavelength, 808 nm; power density, 6 W/cm^2) for different time periods. To determine the impact of NIR power density, the GSPI solution with GS concentration fixed at 50 μg/mL was irradiated under different power densities. The solution temperature was monitored by a thermometer. GO corresponding to the GS concentration at 50 μg/mL was used as positive control, and PBS (pH 7.4) was applied as negative control.

In Vitro Release. For the in vitro release experiment, 0.5 mL portions of GSPID solution in PBS at various pHs (5.0, 6.0, and 7.4) were loaded into dialysis tubes with 8−10 kDa MWCO (Spectrumlabs, U.S.A.). At determined time points, each GSPID solution was irradiated with an 808 nm NIR laser (6 W/cm^2) for 5 min. Aliquots of each 0.5 mL dialysis solution were removed before and after NIR stimulation, and the same volume of fresh corresponding buffer was added back. The amount of released DOX was measured by a fluorescence spectrophotometer for the heat-stimulative release experiment, at determined time points.

Cell Culture. Cells of human glioma cell line, U251, and human astrocyte 1800 cells were obtained from Shanghai Cell Bank, Chinese Academy of Medical Sciences. The cells were maintained in DMEM media supplemented with 10% FBS, 1% L-glutamine, 1% penicillin, and 1% streptomycin stock solutions, at 37 °C and in 5% CO_2. The media were changed every two days, and the cells were passaged by trypsinization before confluence.

Cell Death Imaging. To study the effect of chemotherapy and photothermal therapy, LIVE-DEAD Kits were applied to visualize cell death. U251 cells were cultured in 96-well microplates with 100 μL of media at a density of 1×10^4 cells/well for 24 h. After the cells were washed, GSPI and GSPID with GS concentration at 50 μg/mL were added into the wells, and the cells were incubated for 30 min. For thermal therapy, corresponding wells were irradiated with an 808 nm NIR laser (6 W/cm^2) for 5 min. The culture media was then replaced with fresh media, and the cells were cultured for a further 12 h. After being rinsed carefully, cells were stained by LIVE-DEAD Kits. Confocal images were obtained with a Leica TCs SP5 microscope and the use of a Leica application suite. Live cells exhibited green color, and dead cells showed red color. Repetitive studies were carried out, and three independent fields were examined in each study.

Cell Viability Assay. Cytotoxicity of glioma cells under different treatments was investigated using the CCK-8 assay. First, U251 cells were cultured in 96-well microplates with 100 μL of media at a density of 5×10^3 cells/well for 2 days. GSPI and GSPID with various GS concentrations were each added separately into wells and cultured for 2 h. For thermal therapy, corresponding wells were irradiated with an 808 nm NIR laser (6 W/cm^2) for 5 min. The culture media was then

dx.doi.org/10.1021/ja312221g | J. Am. Chem. Soc. 2013, 135, 4799−4804

replaced with fresh media and cultured for a further 12 h. Then 10 μL of CCK-8 solution was added to each well, and the cells were incubated for another 2 h at 37 °C. After that, the absorbance was measured with a microplate reader at 450 nm. The viability of treated cell wells was expressed as a percentage of the viability of unexposed wells. The combination index (CI) was calculated[30] to evaluate the combination effect of chemotherapy and photothermal therapy. The value of CI represents different meanings, while <1 indicates synergism, >1 means antagonism, and 1 indicates additive effects

Targeting Ability Evaluation in Different Cell Lines. U251 and 1800 cells were respectively cultured in 96-well microplates with 100 μL of media at a density of 5×10^3 cells/well for 2 days. After cells were washed, GSPD and GSPID with GS concentration at 50 μg/mL were added into the cell wells, and the cells incubated for 30 min. The cells were then carefully rinsed two times. Confocal images were obtained for qualitative evaluation, and CCK-8 analysis was performed for quantitative evaluation. The incubation time was extended to 6 h.

■ ASSOCIATED CONTENT

Supporting Information

Further characterization of synthesized GS and GS-based vectors. This material is available free of charge via the Internet at http://pubs.acs.org.

■ AUTHOR INFORMATION

Corresponding Author

rqhuang@fudan.edu.cn

Notes

The authors declare no competing financial interest.

■ ACKNOWLEDGMENTS

This work was supported by the grants from "Zhuo Xue" Talent Plan of Fudan University, "Chen Guang" project supported by Shanghai Municipal Education Commission and Shanghai Education Development Foundation, and National Key Basic Research Program (2013CB932502) of China (973 Program).

■ REFERENCES

(1) Huse, J. T.; Holland, E. C. *Nat. Rev. Cancer.* **2010**, *10*, 319.
(2) Morris, P. G.; Lassman, A. B. *Nat. Rev. Clin. Oncol.* **2010**, *7*, 428.
(3) Sorensen, A. G.; Batchelor, T. T.; Wen, P. Y.; Zhang, W. T.; Jain, R. K. *Nat. Rev. Clin. Oncol.* **2008**, *5*, 634.
(4) Liu, Z.; Robinson, J. T.; Sun, X.; Dai, H. *J. Am. Chem. Soc.* **2008**, *130*, 10876.
(5) Hu, W.; Peng, C.; Lv, M.; Li, X.; Zhang, Y.; Chen, N.; Fan, C.; Huang, Q. *ACS Nano* **2011**, *5*, 3693.
(6) Bao, H.; Pan, Y.; Ping, Y.; Sahoo, N. G.; Wu, T.; Li, L.; Li, J.; Gan, L. H. *Small* **2011**, *7*, 1569.
(7) Hu, S. H.; Chen, Y. W.; Hung, W. T.; Chen, I. W.; Chen, S. Y. *Adv. Mater.* **2012**, *24*, 1748.
(8) Robinson, J. T.; Tabakman, S. M.; Liang, Y.; Wang, H.; Casalongue, H. S.; Vinh, D.; Dai, H. *J. Am. Chem. Soc.* **2011**, *133*, 6825.
(9) Yang, K.; Zhang, S.; Zhang, G.; Sun, X.; Lee, S. T.; Liu, Z. *Nano Lett.* **2010**, *10*, 3318.
(10) Li, M.; Yang, X.; Ren, J.; Qu, K.; Qu, X. *Adv. Mater.* **2012**, *24*, 1722.
(11) Li, D.; Muller, M. B.; Gilje, S.; Kaner, R. B.; Wallace, G. G. *Nat. Nanotechnol.* **2008**, *3*, 101.
(12) Li, X. L.; Wang, X. R.; Zhang, L.; Lee, S. W.; Dai, H. J. *Science* **2008**, *319*, 1229.
(13) Wang, Z. M.; Wang, W.; Coombs, N.; Soheilnia, N.; Ozin, G. A. *ACS Nano* **2010**, *4*, 7437.
(14) Tasciotti, E.; Liu, X. W.; Bhavane, R.; Plant, K.; Leonard, A. D.; Price, B. K.; Cheng, M. M. C.; Decuzzi, P.; Tour, J. M.; Robertson, F.; Ferrari, M. *Nat. Nanotechnol.* **2008**, *3*, 151.
(15) Wang, Y.; Shi, W.; Song, W. S.; Wang, L.; Liu, X. G.; Chen, J.; Huang, R. Q. *J. Mater. Chem.* **2012**, *22*, 14608.
(16) Wang, J.; Liu, W.; Tu, Q.; Wang, J.; Song, N.; Zhang, Y.; Nie, N.; Wang, J. *Biomacromolecules* **2011**, *12*, 228.
(17) Huang, R. Q.; Ke, W. L.; Han, L.; Li, J. F.; Liu, S. H.; Jiang, C. *Biomaterials* **2011**, *32*, 2399.
(18) Ding, H.; Inoue, S.; Ljubimov, A. V.; Patil, R.; Portilla-Arias, J.; Hu, J.; Konda, B.; Wawrowsky, K. A.; Fujita, M.; Karabalin, N.; Sasaki, T.; Black, K. L.; Holler, E.; Ljubimova, J. Y. *Proc. Natl. Acad. Sci. U S A.* **2010**, *107*, 18143.
(19) Debinski, W.; Gibo, D. M.; Obiri, N. I.; Kealiher, A.; Puri, R. K. *Nat. Biotechnol.* **1998**, *16*, 449.
(20) Madhankumar, A. B.; Slagle-Webb, B.; Wang, X.; Yang, Q. X.; Antonetti, D. A.; Miller, P. A.; Sheehan, J. M.; Connor, J. R. *Mol. Cancer. Ther.* **2009**, *8*, 648.
(21) Hummers, W. S. J.; Offeman, R. E. *J. Am. Chem. Soc.* **1958**, *80*, 1339.
(22) Choucair, M.; Thordarson, P.; Stride, J. A. *Nat. Nanotechnol.* **2009**, *4*, 30.
(23) Fan, X. B.; Peng, W. C.; Li, Y.; Li, X. Y.; Wang, S. L.; Zhang, G. L.; Zhang, F. B. *Adv. Mater.* **2008**, *20*, 4490.
(24) Sun, X.; Liu, Z.; Welsher, K.; Robinson, J. T.; Goodwin, A.; Zaric, S.; Dai, H. *Nano Res.* **2008**, *1*, 203.
(25) Markovic, Z. M.; Harhaji-Trajkovic, L. M.; Todorovic-Markovic, B. M.; Kepić, D. P.; Arsikin, K. M.; Jovanović, S. P.; Pantovic, A. C.; Dramićanin, M. D.; Trajkovic, V. S. *Biomaterials* **2011**, *32*, 1121.
(26) Zhu, J.; Liao, L.; Bian, X. J.; Kong, J. L.; Yang, P. Y.; Liu, B. H. *Small* **2012**, *8*, 2715.
(27) Zhang, Z.; Wang, L.; Wang, J.; Jiang, X.; Li, X.; Hu, Z.; Ji, Y.; Wu, X.; Chen, C. *Adv. Mater.* **2012**, *24*, 1418.
(28) Mok, H.; Veiseh, O.; Fang, C.; Kievit, F. M.; Wang, F. Y.; Park, J. O.; Zhang, M. *Mol. Pharmaceutics* **2010**, *7*, 1930.
(29) Padilla-Parra, S.; Matos, P. M.; Kondo, N.; Marin, M.; Santos, N. C.; Melikyan, G. B. *Proc. Natl. Acad. Sci. U S A.* **2012**, *109*, 17627.
(30) Liu, S. H.; Guo, Y. B.; Huang, R. Q.; Li, J. F.; Huang, S. X.; Kuang, Y. Y.; Han, L.; Jiang, C. *Biomaterials* **2012**, *33*, 4907.
(31) Sanchez, V. C.; Jachak, A.; Hurt, R. H.; Kane, A. B. *Chem. Res. Toxicol.* **2012**, *25*, 15.
(32) He, Q.; Zhang, J.; Chen, F.; Guo, L.; Zhu, Z.; Shi, J. *Biomaterials* **2010**, *31*, 7785.
(33) Singh, S. K.; Singh, M. K.; Nayak, M. K.; Kumari, S.; Shrivastava, S.; Grácio, J. J.; Dash, D. *ACS Nano* **2011**, *5*, 4987.
(34) Yang, K.; Wan, J.; Zhang, S.; Zhang, Y.; Lee, S. T.; Liu, Z. *ACS Nano* **2011**, *5*, 516.
(35) Singh, S. K.; Singh, M. K.; Kulkarni, P. P.; Sonkar, V. K.; Grácio, J. J.; Dash, D. *ACS Nano* **2012**, *6*, 2731.
(36) Yang, K.; Feng, L.; Shi, X.; Liu, Z. *Chem. Soc. Rev.* **2013**, *42*, 530.
(37) Lu, W.; Melancon, M. P.; Xiong, C.; Huang, Q.; Elliott, A.; Song, S.; Zhang, R.; Flores, L. G.; Gelovani, J. G.; Wang, L. V.; Ku, G.; Stafford, R. J.; Li, C. *Cancer Res.* **2011**, *71*, 6116.
(38) Day, E. S.; Zhang, L.; Thompson, P. A.; Zawaski, J. A.; Kaffes, C. C.; Gaber, M. W.; Blaney, S. M.; West, J. L. *Nanomedicine* **2012**, *7*, 1133.